Pergamon

*Int. J. Solids Structures* Vol. 31, No. 10, pp. 1429–1445, 1994

0020–7683/94 $7.00 + .00

0020–7683(93)E0021–9

# SINTERING OF FINE-GRAINED MATERIALS BY INTERFACE REACTION CONTROLLED GRAIN BOUNDARY DIFFUSION

Z.-Z. Du† and A. C. F. Cocks
Department of Engineering, Cambridge University, Trumpington Street, Cambridge CB2 1PZ, U.K.

(*Received* 27 *April* 1993; *in revised form* 21 *October* 1993)

**Abstract**—This paper extends the two-state variable material model recently proposed by the authors for the sintering of fine-grained ceramic compacts for situations where grain boundary diffusion is the dominant mechanism to include the effects of an interface reaction. The material model has been incorporated into the finite element code ABAQUS and a range of finite element simulations of a porous cylindrical notched specimen loaded in compression are presented for situations where the controlling mechanism for creep and sintering varies from boundary diffusion to interface reaction controlled. The results are compared with recent experimental results and a numerical analysis. The influence of the interface reaction on the development of microstructure is then discussed.

## 1. INTRODUCTION

Powder processing is being increasingly considered as a manufacturing route to produce high-quality ceramic and intermetallic components. If the compact contains agglomerates, or if a toughening phase in the form of fibres or whiskers is introduced into the compact, then differential rates of densification can occur resulting in the development of a residual stress field, which further influences the evolution of microstructure within the component. When a component is hot isostatically pressed (HIPed) constraint of the can may result in non-uniform densification within the body. As a result, the final product can differ from the original component in shape as well as in scale. To predict the shape change, development of residual stress fields and the evolution of microstructure, it is necessary to develop a set of mechanical constitutive equations that adequately described the material response over the full range of stress states experienced in practice.

The authors (Du and Cocks, 1992a) have recently developed a general framework for constitutive models for the sintering of ceramic components, which can be expressed in terms of two internal state variables, which relate to the physically measureable quantities of relative density and grain size. The relationships for densification and deformation were derived from the work of Ashby (1990), Helle *et al.* (1985), McMeeking and Kuhn (1992), Cocks (1993) and Hsueh *et al.* (1986), and the relationships for grain growth were developed from the studies of Hillert (1965), Shewmon (1964), Brook (1969) and Ashby (1990). In previous studies (Du and Cocks, 1990, 1992b; Cocks and Du, 1993), the full range of models were used to analyse the response of inhomogeneous sintering and HIPing bodies to determine those features of the material response which most critically influence the evolution of residual stress fields and microstructure. However, a feature of these models is that it is implicitly assumed that grain boundary diffusion controls the rate of deformation, providing a linear dependence of strain-rate on stress, although the general structure adopted by the authors (Du and Cocks, 1992a) readily permits relationships describing other mechanisms to be incorporated into a finite element code. Examination of the HIP maps for alumina presented by Ashby (1990) reveals that a number of mechanisms could contribute to the rate of deformation through the entire process. In fine-grained materials diffusion can be limited by interface reactions (Burton, 1972; Ashby, 1969) as grain boundaries under these conditions no longer act as perfect sources or sinks for vacancies. This view is supported by a number of experimental studies (McCoy and Wills, 1987; Cannon

† Current address: Materials Department, University of California, Santa Barbara, CA 93106, U.S.A.

*et al.*, 1956; Besson and Abouaf, 1989) on HIPed alumina compacts. Micromechanical models of interface reactions and constitutive laws for the creep deformation of fully dense materials have been developed by Burton (1972), Arzt *et al.* (1973) and more recently by Cocks (1992), while constitutive relationships for densification of a porous solid have been discussed by McCoy and Wills (1987). Other constitutive laws proposed for interface reaction controlled sintering, such as that of Besson *et al.* (1989, 1990, 1992), are generally based on a phenomenological approach involving disposable functions whose form is determined by experiment. More recently, Cocks (1993) has examined the structure of constitutive laws for the sintering of fine-grained materials for situations where power-law creep and grain boundary diffusion are the dominant mechanisms of deformation and densification. The material response is expressed in terms of scalar stress and strain-rate potentials. General bounds have been developed for these potentials which incorporate a description of the coupling between the different mechanisms.

In the present work, we make use of the strain-rate potentials derived by Cocks (1993) and Pan and Cocks (1993) for situations where grain boundary diffusion mechanisms dominate, which incorporates a description of interfacial processes. Cocks (1993) and Pan and Cocks (1993) provide potentials in the limits of grain boundary diffusive flux and interface reaction controlled sintering and described procedures for interpolating between these limits. Here we develop a set of equations based on their potentials and describe the implementation of these models within the finite element program ABAQUS (1989), where we employ a Newton–Raphson scheme in the solution process.

When developing any material model it is important to assess the predictive capability of the model by evaluating the response of non-uniform components where stress and strain gradients can develop and to compare these results with experimental studies. A feature of the present model is that the state variables relate to physically measurable quantities, allowing a direct comparison to be made between theory and experiment. Recently Besson *et al.* (1990) have performed compressive creep tests on circumferentially notched partially sintered cylindrical specimens of alumina. The tests were stopped prior to the attainment of theoretical density and the variation of density within the component was determined. In Section 4 we use the models presented in Section 2 to calculate the response of this type of component and compare the results with the experimental studies of Besson *et al.* (1990). The results of these calculations allow the influence of the interface reaction on the development of microstructure to be evaluated.

## 2. THE MATERIAL MODEL

It proves convenient to divide the sintering process into two stages: during the early stages of sintering, the pores form an interconnected network through the material. This stage is known as stage 1. With the increase of time, the pores pinch off forming an array of isolated pores and stage 2 starts. The transition to stage 2 occurs when the relative density (density of compact/density of fully compacted material) is greater than about 0.9.

If we identify the total strain-rate $\dot{\varepsilon}_{ij}$ with the symmetric part of the deformation-rate tensor then the general structure of the constitutive relationship becomes

$$\dot{\varepsilon}_{ij} = \dot{\varepsilon}^e_{ij} + \dot{\varepsilon}^c_{ij}, \tag{1}$$

where $\dot{\varepsilon}^e_{ij}$ and $\dot{\varepsilon}^c_{ij}$ are the elastic and inelastic (or creep) strain-rates

$$\dot{\varepsilon}^e_{ij} = C_{ijkl}\check{\sigma}_{kl} + \dot{C}_{ijkl}\sigma_{kl} = C_{ijkl}\check{\sigma}_{kl} + \dot{\rho}\frac{\partial C_{ijkl}}{\partial \rho}\sigma_{kl} \tag{2}$$

$$\dot{\varepsilon}^c_{ij} = \dot{\varepsilon}^c_{ij}(\sigma, \rho, L). \tag{3}$$

In these expressions $C_{ijkl}$ is the elastic compliance matrix, $\sigma_{ij}$ represents the true (or Cauchy) stress and $\check{\sigma}_{ij}$ is the Jaumann rate of Cauchy stress. The second term of eqn (2) is included

here for completeness and takes into account the change of the elastic compliance matrix with density. Equations are available for this effect in the literature (Hsueh *et al.*, 1986; Cocks, 1989), but in creep and sintering studies it is generally observed that inclusion of the variation of compliance with time does not significantly influence the results of the analysis (Hsueh *et al.*, 1986; Rides *et al.*, 1989), particularly for situations where the inelastic deformation is large. In our analysis we therefore assume for simplicity that $C_{ijkl}$ remains constant during sintering.

From the inelastic strain-rate of eqn (3), which is a function of the true stress $\sigma$, $\rho$ and $L$, we may determine the densification rate

$$\dot{\rho} = -\rho\dot{\varepsilon}^c_{kk}. \tag{4}$$

The formation is completed by providing expressions for the grain-growth rate

$$\dot{L} = \dot{L}(\rho, L). \tag{5}$$

This structure of constitutive law is applicable to any of the mechanistic models of the sintering process. Within this framework it is possible to select governing equations for the strain-rate and grain-growth rate reflecting the changing mechanisms and the different stages of sintering. It is necessary to note that $\dot{\varepsilon}_{ij}$ in eqn (3) is the overall strain-rate, either controlled by the rate of diffusion or the rate associated with the interface reaction. In the following sub-sections we provide explicit forms for eqns (3) and (5) for the sintering of fine-grained materials for situations where an interface reaction contributes to the material response.

For situations where different mechanisms are involved, it proves convenient to introduce the strain rate potential $\phi$ and scalar stress potential $\varphi$, which are related as follows (Cocks, 1993):

$$\sigma_{ij}\dot{\varepsilon}_{ij} = \phi + \varphi, \tag{6}$$

where $\phi$ is a function of stress and $\varphi$ is a function of strain-rate. The stress $\sigma_{ij}$ and strain-rate $\dot{\varepsilon}_{ij}$ at a material point can then be determined from the stress potential $\varphi$ and strain-rate potential $\phi$, respectively, in the following manner

$$\sigma_{ij} = \frac{\partial \varphi}{\partial \dot{\varepsilon}_{ij}} \tag{7}$$

$$\dot{\varepsilon}_{ij} = \frac{\partial \phi}{\partial \sigma_{ij}}. \tag{8}$$

In the following sub-sections we obtain explicit forms for $\phi$ and $\varphi$ in the limits of grain boundary flux and interface reaction controlled sintering and describe procedures for interpolating between these two limiting cases. For simplicity we neglect the influence of the sintering potential on the material response in this section. Appropriate expressions for the sintering stress are incorporated into the model in Section 3.

### 2.1. *Boundary diffusion controlled sintering*

Following Du and Cocks (1992a), the strain-rate potential for sintering for the situation where grain boundary diffusion is the dominant mechanism is given by

$$\phi_b = \frac{1}{2}\dot{\varepsilon}_{0b}\sigma_0\left(\frac{L_0}{L}\right)^3\left[c_b(\rho)\left(\frac{\sigma_e}{\sigma_0}\right)^2 + f_b(\rho)\left(\frac{3\sigma_m}{\sigma_0}\right)^2\right] \tag{9}$$

for both stages 1 and 2, where the subscript $b$ represents boundary diffusion controlled sintering, $\dot{\varepsilon}_{0b}$ is the strain-rate experienced by a fully dense material of grain-size $L_0$ at a

Table 1. The functions $f(\rho)$ and $c(\rho)$

| Stages | | Boundary diffusion | Interface reaction |
|---|---|---|---|
| 1 | $f$ | $0.54\dfrac{(1-\rho_0)^2}{\rho(\rho-\rho_0)^2}$ | $\dfrac{1}{3}\dfrac{(1-\rho_0)}{\rho^{3/2}\rho_0^{1/2}(\rho-\rho_0)}$ |
| | $c$ | $1.08\dfrac{(1-\rho_0)^2}{\rho(\rho-\rho_0)^2}$ | $\dfrac{1}{3}\dfrac{(1-\rho_0)}{\rho^{3/2}\rho_0^{1/2}(\rho-\rho_0)}$ |
| 2 | $f$ | $3.2\dfrac{(1-\rho)^{1/2}}{\rho}$ | $\dfrac{0.042}{[1-1.53(1-\rho)^{2/3}]^{5/3}}$ |
| | $c$ | $\dfrac{1}{1-2.5(1-\rho)^{2/3}}$ | $\dfrac{1}{[1-1.84(1-\rho)^{2/3}]^{5/3}}$ |

constant uniaxial stress $\dot{\sigma}_0$, $\sigma_m$ is the mean stress $\sigma_m = \frac{1}{3}\sigma_{kk}$, $\sigma_e$ is the von Mises effective stress and $c_b(\rho)$ and $f_b(\rho)$ are dimensionless functions of the relative density, $\rho$, which are given in Table 1, where during the early stage of sintering

$$\frac{f_b(\rho)}{c_b(\rho)} = 0.5. \tag{10}$$

The relationship of eqn (10) is consistent with results from forging experiments on ceramic compacts and implies that there is zero transverse straining during the early stages of a test as the component contracts in the direction of loading (Besson *et al.*, 1990).

The strain-rate can then be determined from the potential of eqn (9) using the following relationship

$$\dot{\varepsilon}_{ij}^c = \frac{\partial \phi_b}{\partial \sigma_{ij}} = \frac{\partial \phi_b}{\partial \sigma_e}\frac{\partial \sigma_e}{\partial s_{ij}} + \frac{1}{3}\frac{\partial \phi_b}{\partial \sigma_m}\delta_{ij}, \tag{11}$$

where $s_{ij}$ are the deviatoric stresses, $\delta_{ij}$ is the Kroneker delta, and $\sigma_e^2 = \frac{3}{2}s_{ij}s_{ij}$.

We find

$$\dot{\varepsilon}_{ij}^c = \frac{\dot{\varepsilon}_{0b}}{\sigma_0}\left(\frac{L_0}{L}\right)^3 [\tfrac{3}{2}c_b(\rho)s_{ij} + 3f_b(\rho)\sigma_m\delta_{ij}]. \tag{12}$$

The effective deviatoric and dilatational strain rates are given by

$$\dot{\varepsilon}_e = \sqrt{\tfrac{2}{3}\dot{\varepsilon}_{ij}\dot{\varepsilon}_{ij}} \tag{13}$$

$$\dot{\varepsilon}_v = \dot{\varepsilon}_{kk}. \tag{14}$$

Combining eqns (9) and (12)–(14) with eqn (6) gives the stress potential

$$\varphi_b = \frac{1}{2}\dot{\varepsilon}_{0b}\sigma_0\left(\frac{L}{L_0}\right)^3\left[\frac{1}{c_b(\rho)}\left(\frac{\dot{\varepsilon}_e}{\dot{\varepsilon}_{0b}}\right)^2 + \frac{1}{f_b(\rho)}\left(\frac{\dot{\varepsilon}_v}{3\dot{\varepsilon}_{0b}}\right)^2\right]. \tag{15}$$

### 2.2. *Interface reaction controlled sintering*

The equations of Section 2.1 arise from a classical description of the diffusion process in which it is assumed that the grain boundaries act as perfect sources and sinks for vacancies. All the work done by the applied load during deformation then goes to drive the diffusive flux of material along the boundaries. In practice, however, the boundaries are not ideal and some of the work must go to drive the sources and sinks. Inclusion of this

feature of the material response is particularly important in fine-grained materials where, because of the short diffusion distances, the rate at which material can be added to, or removed from, a boundary can be the rate controlling stage of the process. In this subsection we examine the situation where the rate of diffusional flow is so fast that virtually all the work done by the applied load is needed to drive the interface reaction.

First we consider stage 1 of sintering when the porosity is open and discrete necks exist between the particles. Cocks (1993) has recently examined this situation using procedures similar to that employed by Kuhn and McMeeking (1992) in the development of their model for isolated contacts of power law creeping particles. Like the model of Kuhn and McMeeking (1992), the model developed by Cocks (1993) is essentially a micromechanical model, having the same structure as that developed by Kuhn and McMeeking (1992). Besson *et al.* (1989, 1990, 1992) on the other hand based the structure of their model on a uniaxial model of a fully dense material proposed by Arzt *et al.* (1973). Their model is essentially an empirical model and no detailed potential form was given, although in the limit of interface reaction controlled sintering their equations can be expressed in terms of a quadratic potential, which is not consistent with the micromechanical model developed by Cocks (1993).

Following Cocks (1993), the strain-rate potential $\phi_r$ for stage 1 can be written in the following general form

$$\phi_r = \frac{1}{3}\dot{\varepsilon}_{0r}\sigma_0\frac{L_0}{L}\left[c_r(\rho)\left(\frac{\sigma_e}{\sigma_0}\right)^{3/2} + f_r(\rho)\left(\frac{|3\sigma_m|}{\sigma_0}\right)^{3/2}\right]^2, \tag{16}$$

where the subscript $r$ indicates that an interface reaction controls the deformation rate.

As noted above, in uniaxial forging experiments there is zero lateral strain as the material densifies in the early stages of sintering. This suggests that

$$\frac{f_r(\rho)}{c_r(\rho)} = 0.5 \tag{17}$$

during stage 1.

By examining the analysis of Cocks (1993), the detailed functions $c_r(\rho)$ and $f_r(\rho)$ can be determined as given in Table 1, where we have adjusted the numerical constant for the functional form of $c_r(\rho)$ from that originally proposed by Cocks (1993) to force eqn (17) to hold. In the original formalism proposed by Cocks (1993), $c_r(\rho)$ is a factor of 1.84 larger, giving $f_r(\rho)/c_r(\rho) = 0.27$.

Differentiating $\phi_r$ of eqn (16) with respect to $\sigma_e$ and $\sigma_m$, respectively, gives the effective deviatoric and dilatational strain-rates.

$$\dot{\varepsilon}_e = \dot{\varepsilon}_{0r}\left(\frac{L_0}{L}\right)c_r(\rho)\left[c_r(\rho)\left(\frac{\sigma_e}{\sigma_0}\right)^{3/2} + f_r(\rho)\left(\frac{|3\sigma_m|}{\sigma_0}\right)^{3/2}\right]\sqrt{\frac{\sigma_e}{\sigma_0}} \tag{18}$$

$$\dot{\varepsilon}_v = 3.0\dot{\varepsilon}_{0r}\left(\frac{L_0}{L}\right)f_r(\rho)\left[c_r(\rho)\left(\frac{\sigma_e}{\sigma_0}\right)^{3/2} + f_r(\rho)\left(\frac{|3\sigma_m|}{\sigma_0}\right)^{3/2}\right]\left(\frac{3\sigma_m}{\sigma_0}\right)\sqrt{\frac{\sigma_0}{|3\sigma_m|}}. \tag{19}$$

The stress potential obtained from eqn (6) is then

$$\varphi_r = \frac{2}{3c_r(\rho)f_r(\rho)}\dot{\varepsilon}_{0r}\sigma_0\sqrt{\frac{L}{L_0}}\sqrt{f_r^2(\rho)\left(\frac{\dot{\varepsilon}_e}{\dot{\varepsilon}_{0r}}\right)^3 + c_4^2(\rho)\left|\frac{\dot{\varepsilon}_v}{3\dot{\varepsilon}_{0r}}\right|^3}. \tag{20}$$

Pan and Cocks (1993) give the appropriate potential for stage 2 as

$$\phi_r = \frac{1}{3}\dot{\varepsilon}_{0r}\sigma_0 \frac{L_0}{L}\left[c_r(\rho)\left(\frac{\sigma_e}{\sigma_0}\right)^{2.5} + f_r(\rho)\left(\frac{|3\sigma_m|}{\sigma_0}\right)^{2.5}\right]^{1.2} \tag{21}$$

The functions $c_r(\rho)$ and $f_r(\rho)$ are again given in Table 1.

Following the procedure described above for stage 1, we obtain the dual potential

$$\varphi_r = \frac{2}{3}\dot{\varepsilon}_{0r}\sigma_0\sqrt{\frac{L}{L_0}}\left[c_r^{-2/3}(\rho)\left(\frac{\dot{\varepsilon}_e}{\dot{\varepsilon}_{0r}}\right)^{5/3} + f_r^{-2/3}(\rho)\left|\frac{\dot{\varepsilon}_v}{3\dot{\varepsilon}_{0r}}\right|^{5/3}\right]^{0.9}. \tag{22}$$

2.3. *The coupled problem*

In the last two sub-sections, we presented the detailed forms of the scalar stress and strain-rate potentials when the deformation is solely controlled by boundary diffusion or an interface reaction. In practice, the deformation and densification processes may be controlled by a combination of these two different mechanisms. In this sub-section we construct the equations for the scalar stress and strain-rate potentials for intermediate strengths of the interface reaction, from which a set of equations which relate the stresses, strain rates and other state variables are developed.

According to Cocks (1993), an upper bound for the scalar stress potential for the coupled problem is given by

$$\varphi = \varphi_b + \varphi_r. \tag{23}$$

Here we assume that eqn (23) provides an accurate description of the stress potential and employ eqn (24) to determine the corresponding strain-rate potential

$$\phi = \sigma_{ij}\dot{\varepsilon}_{ij} - \varphi = \sigma_m\dot{\varepsilon}_v + \sigma_e\dot{\varepsilon}_e - \varphi. \tag{24}$$

These equations simply reflect the fact that the two processes are sequential, i.e. both must operate at equivalent rates. The response is then equivalent to two parallel viscous elements within a rheological model, with one element representing the diffusive flux of material and the other reflecting the operation of the sources and sinks. Cocks and Pan (1993) discuss this type of rheological model in more detail.

Substituting $\varphi_b$ of eqn (15) and $\varphi_r$ of eqns (20) and (22) respectively into eqn (23) we can then obtain the scalar stress potential for the coupled problem for both stages 1 and 2.

The stresses can then be determined using eqn (7), i.e.

$$\sigma_m = \frac{\partial\varphi}{\partial\dot{\varepsilon}_v} \tag{25}$$

$$\sigma_e = \frac{\partial\varphi}{\partial\dot{\varepsilon}_e}. \tag{26}$$

The strain-rate potential can again be obtained by combining eqns (25) and (26) with eqn (24), but this requires inversion of eqns (25) and (26) to express the strain rates in terms of the applied stress. This cannot be achieved analytically, and in the following section we employ a Newton–Ralphson scheme to perform these tasks.

For the conditions employed in Coble's (1963) sintering experiments Du and Cocks (1992a) determined that grain growth is limited by the mobility of the pores. The appropriate equations for the grain growth rate of eqn (5) are then

$$\dot{L} = \dot{L}_0 \left(\frac{L_0}{L}\right)^3 (1-\rho)^{-3/2} \tag{27}$$

$$\dot{L} = \dot{L}_0 \left(\frac{L_0}{L}\right)^3 (1-\rho)^{-4/3} \tag{28}$$

for stage 1 and 2, respectively, where $\dot{L}_0$ is a material constant.

To smooth the computational process, a transition period ($\rho_1 < \rho < \rho_2$) was introduced between stages 1 and 2. The strain-rate potential $\phi_t$ and the grain growth rate $\dot{L}_t$ during this stage were taken as

$$\phi_t = k\phi_{\text{stage 1}} + (1-k)\phi_{\text{stage 2}} \tag{29}$$

$$\dot{L}_t = kL_{\text{stage 1}} + (1-k)\dot{L}_{\text{stage 2}}, \tag{30}$$

where

$$k = \frac{\rho_2 - \rho}{\rho_2 - \rho_1},$$

in order to provide a gradual transition from stage 1 to stage 2. Following Ashby (1990) and Fleck *et al.* (1992), values of $\rho_2 = 0.95$ and $\rho_1 = 0.9$ were chosen.

We now have equations for densification and deformation [eqns (25) and (26)] and grain growth [eqns (27) and (28)] for both stages of sintering. It is necessary to note that in the development of the constitutive model, various material parameters $\dot{\varepsilon}_{0b}$, $\dot{\varepsilon}_{0r}$, $\dot{L}_0$ and $\sigma_0$ were introduced. In previous work, Du and Cocks (1992a) determined the values of these quantities when interfacial processes were neglected by fitting each model to the experimental data of Coble (1963), who conducted sintering experiments on fine-grained compacts of alumina with an initial grain size of 0.3 $\mu$m at 1480°C. The values of these quantities are

$$\dot{\varepsilon}_{0b} = 6.85 \times 10^{17} \frac{\exp(-7.698 \times 10^4/T)}{T}$$

and

$$\dot{L}_0 = 3.15 \times 10^{12} \frac{\exp(-7.698 \times 10^4/T)}{T}$$

for $\sigma_0 = \gamma/L_0$, where $\gamma$ is the surface free energy per unit area. In the analyses presented in the following sections where the initial grain size is allowed to vary the values of $\dot{\varepsilon}_{0b}$, $\dot{L}_0$ and $\sigma_0$ were adjusted accordingly. In the present work, we assume the values of these quantities are still valid and define a dimensionless parameter $\alpha$ which compares the rate of grain boundary diffusion with the rate associated with the interface reaction

$$\alpha = \frac{\dot{\varepsilon}_{0b}}{\dot{\varepsilon}_{0r}} \tag{31}$$

which is similar to that originally proposed by Cocks (1992). In the situations considered in this paper the absolute values of $\dot{\varepsilon}_{0b}$, $\dot{L}_0$ and $\sigma_0$ play only a minor role in determining the stress state and microstructure within a component for a prescribed applied displacement. The component response can effectively be described in terms of the quantity $\alpha$ defined in eqn (31). When $\alpha$ is much greater than 1, the rate of diffusion is much faster than the rate associated with the interface reaction, and since the slower process governs the overall rate,

the material response is interface reaction controlled. Similarly if $\alpha \ll 1$, the interface reaction occurs at a fast rate and the rate of material transport is controlled by diffusion. For intermediate values of $\alpha$ both boundary diffusion and the interface reaction contribute to the overall rate of deformation. We examine this point further in the following section when we analyse the response of a porous ceramic notched compact under compressive creep loading.

## 3. NUMERICAL ANALYSIS AND FINITE ELEMENT MODELS

In this section we implement the material model of Section 2 using the commercial finite element code ABAQUS (1989) through the user-defined CREEP subroutine, with the relative density and grain size treated as solution-dependent state variables. This routine allows any creep laws of the general form

$$\dot{\varepsilon}_e = g(\sigma_m, \sigma_e, \varepsilon_v, \varepsilon_e, \ldots) \tag{32}$$

$$\dot{\varepsilon}_v = g(\sigma_m, \sigma_e, \varepsilon_v, \varepsilon_e, \ldots) \tag{33}$$

to be defined.

If we include the sintering potential in the constitutive equations presented in Section 2, eqn (25) becomes

$$\sigma_m - \sigma_s = \frac{\partial \varphi}{\partial \dot{\varepsilon}_v}, \tag{34}$$

where the sintering potential (Ashby, 1990)

$$\sigma_s = \frac{\gamma}{0.06L}\rho^2(2\rho - 0.64) \tag{35}$$

for stage 1, and

$$\sigma_s = \frac{4\gamma}{L}\left(\frac{1-\rho}{6}\right)^{-1/3} \tag{36}$$

for stage 2.

It is evident that the forms of these equations [eqns (26) and (34)] are different to those described in ABAQUS with the stresses expressed as a non-linear function of the strain-rate. Inversion of these relationships is best performed using a Newton–Raphson scheme. The detailed procedure adopted in this study is presented in the Appendix.

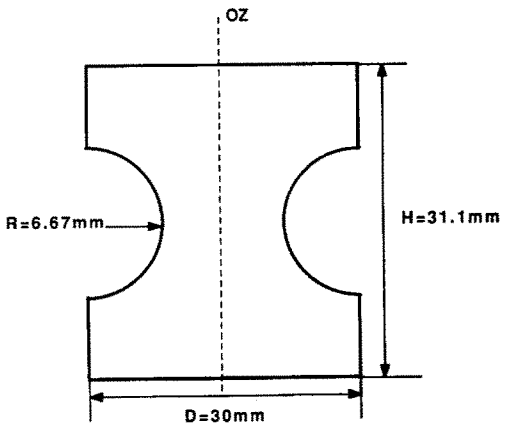


Fig. 1. Geometry of the notched specimen.

Recently Besson *et al.* (1990) have performed a series of compressive creep tests on samples of 99.98% alumina. Cylindrical samples were initially hot pressed to relative densities between 0.74 and 0.92 to provide enough strength for circumferential notches to be machined in the specimens. The geometry of the notched samples is illustrated in Fig. 1, which had a height of 31.10 mm, a diameter of 30 mm and a notch radius of 6.67 mm. The notched samples were repressed for a period of time, with the test stopped before the samples had reached full density. The variation of density within a specimen was then determined by microhardness tests, and by measuring the X-ray absorption characteristics, at various sections. Here we analyse one particular test for which a complete set of data is available. Initially, the sintering body had a uniform grain size of 0.25 $\mu$m and a relative density of 0.744. A constant load giving a mean applied stress, $\sigma_n$ of 15 MPa was applied at the top of the specimen and the temperature was maintained constant at 1270°C. The test was stopped when the specimen had reduced in height from 31.1 to 28.16 mm.

A finite element mesh was constructed for a quarter of the specimen of Fig. 1 using the finite element mesh generator FEMGEN (FEMVIEW, 1989). For the present problem, where the dilatational strain-rates remain quite substantial throughout the solution process a number of types of element can be used. In this situation the use of axisymmetric eight-noded isoparametric elements with reduced integration stations, provides the best balance between economy and accuracy. The formulation for these models was implemented using the commercial finite element code, ABAQUS (1989) mounted on a Sun Workstation. The creep user-interface described above was used with both grain size and relative density considered as solution-dependent state variables. Automatic time increments associated with the implicit creep integration scheme were used as this is generally more effective for large time-dependent problems.

In the present work, the elastic Young's modulus at full density, $E = 133$ GPa was used throughout the whole process of sintering, and Possion's ratio was set to 0.33. The tolerance was chosen to be less than 0.1% of the typical applied force. The computation was stopped when the calculated height of the cylinder achieved the experimental value of 28.16 mm. The distribution of the hydrostatic pressure, relative density and the average grain size inside the cylinder were then determined. Typical solution times for each iteration were of the order of 0.15 s. The total solution time for a problem to achieve the calculated height of the cylinder was approximately 2 h.

## 4. COMPARISON BETWEEN FINITE ELEMENT COMPUTATIONS AND EXPERIMENTAL DATA

In a previous study (Du and Cocks, 1991), a range of material models were used to examine the response of the notched component described above. All these models were linear viscous in character and offer different descriptions of the material response for situations where the grain boundaries act as perfect sources and sinks for vacancies and grain boundary diffusion was the only mechanism responsible for deformation and densification ($\alpha = 0$). Before examining the material response when an interface reaction is included, it is instructive to examine the major factors which were identified as being important in determining the predicted response of the component in Du and Cocks (1991). These are: the relative magnitudes of the shear and dilatational strain-rate [measured by the ratios of $f_b/c_b$ and $(\sigma_m - \sigma_s)/\sigma_e$] and the magnitude of the sintering potential compared to the applied stress $\sigma_s/\sigma_n$.

In general, the larger the ratio $f_b/c_b$, the higher the density and the higher the density gradient within the compact, with the magnitude of the stresses generally increasing with increasing values of $f_b/c_b$. Two sets of calculations were performed; the sintering potential was either set equal to zero or eqns (35) and (36) were employed. It was found that using eqn (35), a sintering potential in the range 30–73 MPa is predicted over the range of densities found experimentally for a grain size of 0.25 $\mu$m. These values are much greater than the applied stress $\sigma_n$ of 15 MPa. As a result, the sintering potential becomes the dominant factor in determining the densification rate, resulting in significant lateral contraction and reasonably uniform strain-rate and density distributions. However, if the sintering potential

is set to zero, lower density levels were evident for all the material models, which are much closer to the experimental results of Besson *et al.* (1990).

Other factors, such as the detailed form of the functions $f_b(\rho)$ and $c_b(\rho)$ and the extent of grain growth played relatively minor roles in determining the evolution of microstructure. In all the computer simulations of Besson *et al.*'s (1990) experiments, no part of the component had entered stage 2 up to the end of the test. As a result there is a fairly uniform distribution of grain size in the component; it had increased by a maximum of 27% when the analysis was terminated.

When the sintering potential of eqn (35) is employed, the component creeps and densifies at a uniform rate and the detailed forms of $f_b(\rho)$ and $c_b(\rho)$ have little influence on the component response. A greater sensitivity is observed when the sintering potential is set equal to zero. When a notched component is compressed the material across the minimum section initially densifies much quicker than material in the bulk of the component. As it densifies further it becomes more creep resistant and a more uniform densification rate is observed in the component. For the material models in which $f_b(\rho)$ and $c_b(\rho)$ are the most sensitive to density, the material hardens quicker across the minimum section, slowing down the rate of densification, and allowing a more uniform distribution of density to develop within the component, and since the overall displacement is prescribed, the mean density across the minimum section is less than that obtained for the models where the bulk and shear viscosities vary less with density.

In the present work, the same problem has been analysed for the material model described in Section 3 with the value of $\alpha$ varied from 0 to $\infty$, which implies that deformation and densification changes from boundary diffusion controlled to interface reaction controlled. We again present the results from two sets of calculations: the sintering potential was either set to zero, or the relationships of eqns (35) and (36) were employed. To provide further insight into this class of problem, computations have also been performed for situations where the ratio $f_r/c_r$ for the material model has been arbitrarily changed. This involves reducing $f_r/c_r$ by a factor of 1.86 to yield a value of $f_r/c_r = 0.26$ during stage 1, which is the ratio originally obtained by Cocks (1993) from his bounding calculations. By examining the results of these different calculations we can determine the influence of the ratio of these two quantities and the functional forms for the sintering potential on the evolution of microstructure within the compact when the sintering process is controlled by a combination of two different mechanisms.

Similar to the results presented in Du and Cocks (1991) the entire component remained in stage 1 up to the termination of the test for all the problems analysed. As a result, we limit our attention to the material response in stage 1. Figures 2 and 3 provide a comparison of the density distribution obtained experimentally with the finite element predictions for a range of values of $\alpha$ when eqn (35) is used for the sintering potential in stage 1 and both $f_b/c_b$ and $f_r/c_r$ equal 0.5. For a given value of $\alpha$, it is found that the density is larger in the regions close to the notch than those remote from it, with the maximum relative density occurring at the notch tip. This is due to the fact that the material densifies faster at the notch root initially, driven by the high initial elastic mean stress in this region. As the

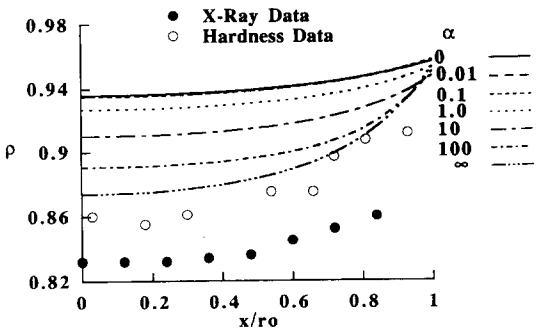


Fig. 2. A comparison of the radial density profile in the notched region of the specimen between the experimental data and the current results, in which the sintering potential is evaluated using eqn (35) when both $f_b/c_b$ and $f_r/c_r$ equal 0.5.

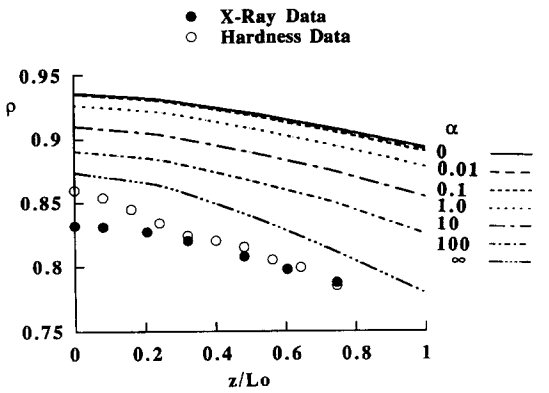


Fig. 3. A comparison of the axial density profile along the $OZ$ axis in the notched region of the specimen between the experimental data and the current results, in which the sintering potential is evaluated using eqn (35) when both $f_b/c_b$ and $f_r/c_r$ equal 0.5.

material densifies it becomes more creep resistant and in order for the material to densify at a rate that is compatible with the surrounding less dense material the mean stress at the notch must increase in magnitude much faster than in the bulk of the component.

Examination of these figures also reveals that the higher the value of $\alpha$, the steeper the density gradients in the compact as a result of the smaller lateral contraction observed as the interface reaction becomes stronger (large $\alpha$). The levels at the density, however, decrease with increasing $\alpha$ with the results lying closer to the experimental data when $\alpha \to \infty$, reflecting the fact that the ratio of the dilatational strain rate to the effective deviatoric strain rate ($\dot{\varepsilon}_v/\dot{\varepsilon}_e$) decreases with increasing $\alpha$ (Fig. 4). When the sintering process is dominated by the boundary diffusion process this ratio is largely determined by the ratio $3(\sigma_m-\sigma_s)/\sigma_e$, while it is proportional to $\sqrt{3}(|\sigma_m-\alpha_s|)/\sigma_e$ when sintering is controlled by an interface reaction. If the sintering potential of eqn (35) is used throughout stage 1, the sintering potential is much larger than the applied mean stress. As a result, the ratio of the dilatational strain rate to the deviatoric strain rate is much larger when sintering is controlled by boundary diffusion than when it is controlled by an interface reaction.

Another possible factor that could play an important role in determining the density profile is the sensitivity of the material response to the relative density, and how this varies as $\alpha$ is increased. When sintering is controlled by an interface reaction, the strain-rates are proportional to $f_r^2$ and $c_r^2$, while in the diffusion limit, they are proportional to $f_b$ and $c_b$. The way in which these quantities vary with relative density is shown in Fig. 5. The plots for $f_b$ and $f_r^2$ and $c_b$ and $c_r^2$ are very similar and the slight variations that are evident from these plots is likely to have a negligible effect on the density profile in the body.

It is evident from the above discussion that the key to understanding the development of microstructure within a component is provided by examining the factors that influence the ratio $\dot{\varepsilon}_v/\dot{\varepsilon}_e$. In the above example we employed a certain structure for the constitutive relationships and a particular expression for the sintering potential. Further insight into

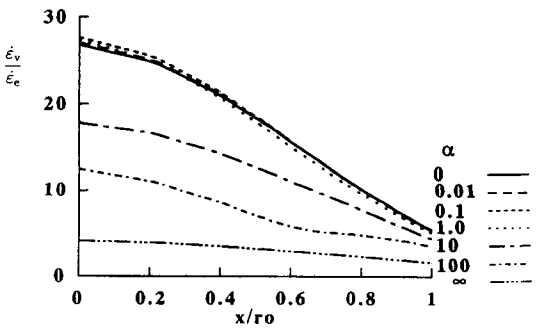


Fig. 4. A comparison of the ratio of dilatational and deviatoric strain-rate along the minimum section for a range of $\alpha$ values.

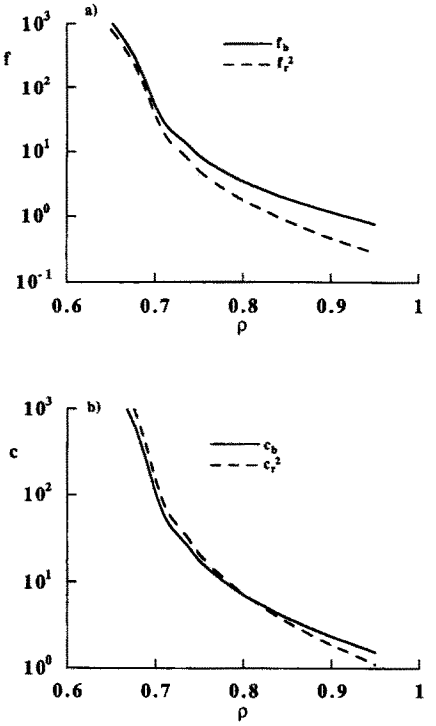


Fig. 5. Comparison of (a) $f$ as a function of relative density and (b) $c$ as a function of relative density for the different mechanisms at stage 1.

the component response can be obtained by examining the effect of changing these relationships. First we consider the effect of changing $f_r$, such that $f_r/c_r = 0.27$. The resulting variation of density across the minimum section and along the axis of the component are shown in Figs 6 and 7.

It is evident that these results exhibit the same trend as observed when $f_r/c_r = 0.5$ and $f_b/c_b = 0.5$. When $\alpha$ is less than 1, both sets of results are similar to those obtained when $f_r/c_r = 0.5$, as in this regime, boundary diffusion dominates the process of sintering and the variation of $f_r/c_r$ has little effect on the overall density distribution in the compact. However, when $\alpha$ is larger than 1, significant differences are observed, with the levels of density and density gradients being smaller for smaller values of $f_r/c_r$. Reducing $f_r$, reduces the ratio of $\dot{\varepsilon}_v/\dot{\varepsilon}_e$ on average in the body, giving larger transverse displacements and less densification. This result is consistent with those presented in Du and Cocks (1991) when $\alpha = 0$ and the ratio $f_b/c_b$ was varied. It was observed that the larger the ratio of $f_b/c_b$, the higher the density level and density gradients.

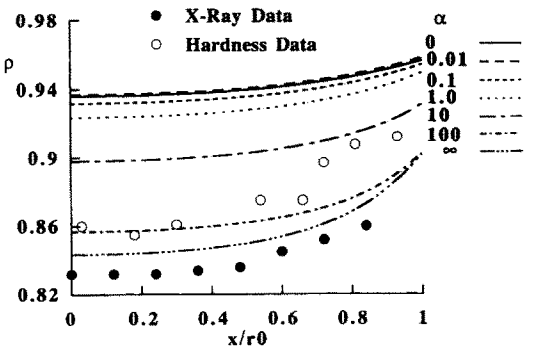


Fig. 6. A comparison of the radial density profile in the notched region of the specimen between the experimental data and the current results, in which the sintering potential is evaluated using eqn (35) when $f_b/c_b = 0.5$ and $f_r/c_r = 0.27$.

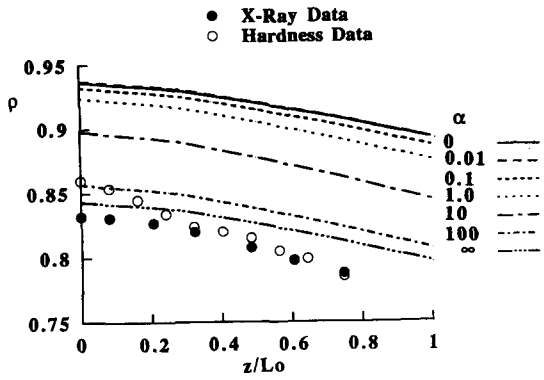


Fig. 7. A comparison of the axial density profile along the $OZ$ axis in the notched region of the specimen between the experimental data and the current results, in which the sintering potential is evaluated using eqn (35) and both $f_b/c_b = 0.5$ and $f_r/c_r = 0.27$.

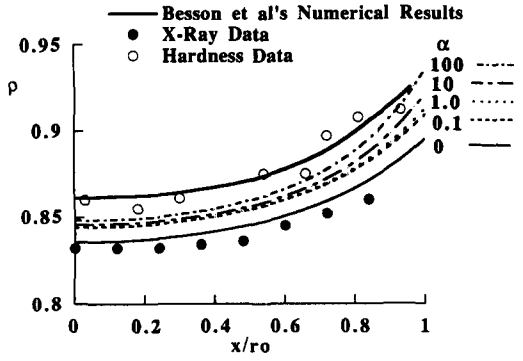


Fig. 8. A comparison of the radial density profile in the notched region of the specimen between the experimental data and the current results, in which the sintering potential is set to zero when both $f_b/c_b$ and $f_r/c_r$ equal 0.5.

In the above examples the component response is largely determined by the magnitude of the sintering potential. In order to more fully examine the influence of other features of the material model a set of computations were performed in which the sintering potential was set to zero, with $f_r/c_r$ and $f_b/c_b$ both equal to 0.5.

The variation of density across the minimum section and along the axis of the specimen obtained from the computations are compared with the experimental data of Besson *et al.* (1990) in Figs 8 and 9. To provide further insight into this class of problem the numerical results obtained by Besson *et al.* (1990) using an empirical model are illustrated alongside the

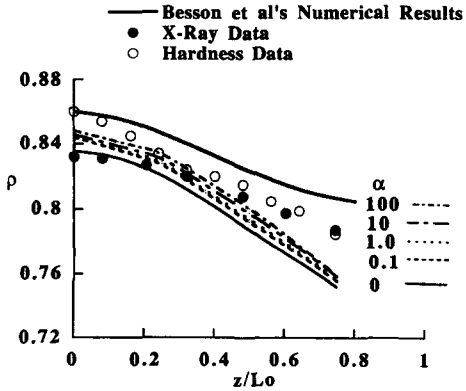


Fig. 9. A comparison of the axial density profile along the $OZ$ axis in the notched region of the specimen between the experimental data and the current results, in which the sintering potential is set to zero and both $f_b/c_b$ and $f_r/c_r$ equal 0.5.

current computational results. Examination of Figs 8 and 9 reveals that lower density levels and sharper density gradients are evident in comparison with the results of Figs 3 and 4. Also the lateral contraction is much smaller in comparison with that when the sintering potential of eqn (35) was employed. Examination of these results also indicates that the larger the value of $\alpha$ the higher the level of density. This is a direct result of the non-linear nature of the constitutive relationship in the limit of interface reaction controlled sintering. As $\alpha$ is increased the strain becomes more concentrated across the minimum section of the component, resulting in a higher local density for a given imposed axial displacement. The differences between the densities arising from the variation of $\alpha$ are smaller when $\sigma_s = 0$ than when the sintering potential of eqn (35) was employed. All the results lie in a tight band between the two sets of experimental data provided by Besson *et al.* (1990). An interesting feature of these results is that the level of the density increases and approaches the numerical prediction of Besson *et al.* (1990) as $\alpha$ increases. If the grain size is set to a constant value of 0.25 $\mu$m and the values of the creep constants determined by fitting the experimental data (Besson *et al.*, 1990) are used, we find that Besson *et al.*'s (1990) empirical equation leads to a value of $\alpha$ of the order of 100.

## 5. DISCUSSION

In the present paper we have extended a two-state variable material model recently proposed by the authors (Du and Cocks, 1992a) for the sintering of fine-grained ceramic compacts for situations where grain boundary diffusion is the dominant mechanism to include the effects of an interface reaction. A range of finite element simulations of a porous ceramic notched component have been performed. The major aims of this study were to assess the predictive capability of the material model and to determine those features of the model that most influence the response of a sintering component when the effect of an interface reaction is included.

As with previous studies (Du and Cocks, 1991, 1992b) it is found that the expressions employed for the sintering potential and the ratios of $f/c$ play the most significant roles in determining the development of microstructure in the body. For the range of conditions examined here eqns (35) and (36) predict values of the sintering potential that are much larger than the applied stress of 15 MPa. These large values tend to dominate the response of the component. In the limit of diffusion controlled sintering the higher sintering potential causes the body to densify at an almost uniform rate, giving large lateral contractions and the highest densities for a given axial displacement (Fig. 2). When an interface reaction operates the sintering potential also influences the deviatoric strain-rates as a result of the non-linear nature of the constitutive law [see eqn (18) with $\sigma_m$ replaced by $\sigma_m - \sigma_s$]. As a result the extent of lateral contraction decreases with increasing strength of the interface reaction, giving lower density levels for a given axial displacement (Fig. 2).

When the sintering potential is assumed to be much less than the axial stress there is less variation in the results and the opposite trend to that described above is observed as the strength of the interface reaction is increased (Fig. 8). Suppressing the sintering potential results in a wider variation of strain and densification rate within the body. The increasing non-linear nature of the material response as the strength of the interface reaction increases, results in a stronger localization of the strain across the minimum section and higher local density levels.

Examination of Figs 2, 3, 8 and 9 reveals that the computational results lie within the experimental data at large $\alpha$, independent of the choice of the expression for the sintering potential. Besson *et al.*'s (1990) data and empirical model suggest that $\alpha$ is of the order of 100 for the range of condition employed in their experiments. It is useful to examine this limit in more detail.

First consider a test in uniaxial compression, where the specimen is subjected to a constant axial stress $\sigma$. If $\dot{\varepsilon}_a$ is the axial strain rate and $\dot{\varepsilon}_T$ the transverse strain rate then [from eqns (18) and (19)]

$$\frac{\dot{\varepsilon}_T}{\dot{\varepsilon}_a} = \frac{\frac{f_r}{c_r}\sqrt{\left(1+\frac{3\sigma_s}{\sigma}\right)}-0.5}{\frac{f_r}{c_r}\sqrt{\left(1+\frac{3\sigma_s}{\sigma}\right)}+1}. \tag{37}$$

Besson *et al.* (1990) observed that $\dot{\varepsilon}_T = 0$ during stage 1 sintering in their uniaxial compression tests. In the development of the material constitutive relationships we assume that the level of stress used in these tests was such that $\sigma_s \ll \sigma$, giving $f_r/c_r = 0.5$. If, however, $\sigma_s$ was of the order of $\sigma$ then $f_r/c_r = 0.25$ would have been a more appropriate choice, which is close to the original value proposed by Cocks (1993) from his bounding calculations. In the computations for $f_r/c_r = 0.27$, presented in Figs 6 and 7, the sintering potential was of the order of the mean stress across the minimum section of the notched component throughout the sintering process. If we compare the results for $\alpha \to \infty$ on Figs 6 and 8 (i.e. $f_r/c_r = 0.27$ and $\sigma_s = \sigma_{\text{net}}$ with $f_r/c_r = 0.5$ and $\sigma_2 = 0$) we observe that the mean densities across the minimum section are comparable, with a wider variation of density observed when $\sigma_s = 0$. This result serves to illustrate the major points of this paper. Provided the uniaxial data are adequately described by the constitutive model, i.e. the ratio $\dot{\varepsilon}_v/\dot{\varepsilon}_e$ is accurately predicted, then the correct magnitude of the density is obtained from the computations. In situations where the sintering potential is large, smaller variations of density are observed in the body, but the density profile still lies within the scatter band of experimental results.

Other factors, such as the detailed form of the functions $f_r(\rho)$ and $c_r(\rho)$ play relatively minor roles in determining the evolution of microstructure (Figs 8 and 9). At a given value of $\alpha$, provided the current model adequately fits the same data as Besson *et al.*'s model (1989, 1990, 1992), it will give largely the same results.

It is evident from the above discussion that the key to fully understanding the development of microstructure during sintering lies in obtaining an accurate description of the sintering potential. There is no universally accepted set of expressions for this potential. In situations where values have been obtained experimentally, it has been found to lie in the range of 1–2 MPa (Hsueh *et al.*, 1986; Rahaman *et al.*, 1986). The grain size employed in these studies was, however, larger than that considered here. Equations (35) and (36) suggest that the sintering potential decreases with increasing grain size, so we might expect higher values than the oft quoted value of 1 MPa, although the magnitudes of the sintering potential obtained here are far in excess of this value. Clearly, future development of the constitutive models requires more accurate expressions for the sintering potential and further detailed experiments on a range of engineering components of the type described by Besson *et al.* (1990) to fully evaluate and calibrate these models.

*Acknowledgements*—This research was supported by the Science Engineering Research Council under Grant No. GR/G42181, and by a contract (N00014-91-J-4089) with the Defence Advanced Research Projects Agency and the Office of Naval Research through a collaborative programme with the University of Virginia. Thanks are due to Hibbitt, Karlsson and Sorensen, Inc. for access to ABAQUS under academic licence.

## REFERENCES

ABAQUS (1989). Hibbitt, Karlsson and Sorensen Inc., ABAQUS user manual.

Arzt, E., Ashby, M. F. and Verall, A. (1983). Interface controlled diffusional creep. *Acta Metall.* **31,** 1977–1989.

Ashby, M. F. (1969). On interface-reaction control of Narbarro–Herring creep and sintering. *Scripta Metall.* **3,** 837–842.

Ashby, M. F. (1990). Background reading, HIP 6.0. University of Cambridge.

Besson, J. and Abouaf, M. (1989). Finite element simulations of hot isostatic pressing of ceramic powders. *Proceedings of the Second International Conference on Hot Isostatic Pressing—Theory and Application.* Gaitherburg.

Besson, J. and Abouaf, M. (1992). Rheology of porous alumina and simulation of hot isostatic pressing. *J. Am. Ceramic Soc.* **75,** 2165–2172.

Besson, J., Abouaf, M., Mazerolle, F. and Suquet, P. (1990). Compressive creep tests on porous ceramic notched specimens. *IUTAM Symposium on Creep in Structures.* Krakow.

Brook, R. J. (1969). Pore–grain boundary interactions and grain growth. *J. Am. Ceramic Soc.* **52,** 56–57.

Burton, B. (1972). Interface reaction controlled diffusional creep: a consideration of grain boundary dislocation climb sources. *Material Sci. Engng* **10,** 9–14.

Cannon, R. M., Rhodes, W. H. and Heuer, A. H. (1980). Plastic deformation of fine grained alumina I interface-controlled diffusional creep. *J. Am. Ceramic Soc.* **63,** 46–53.
Coble, R. L. (1963). Sintering crystalline solids, II experimental test of diffusion models in powder compacts. *J. appl. Phys.* **32,** 793.
Cocks, A. C. F. (1989). Inelastic deformation of porous materials. *J. Mech. Phys Solids* **37,** 693–715.
Cocks, A. C. F. (1992). Interface reaction controlled creep. *Mechanics of Materials* **13,** 165–174.
Cocks, A. C. F. (1993). The structure for constitutive laws for the sintering of fine grained materials. To be published.
Cocks, A. C. F. and Du, Z.-Z. (1993). Pressureless sintering and HIPing of inhomogeneous ceramic compacts. *Acta Metall.* **41,** 2113–2126.
Cocks, A. C. F. and Pan, J. (1993). To appear.
Du, Z.-Z. and Cocks, A. C. F. (1990). A finite element analysis for an inhomogeneous $Al_2O_3$ sintering body. *Proceedings of the 6th U.K. ABAQUS Group Meeting.* Manchester.
Du, Z.-Z. and Cocks, A. C. F. (1991). A finite element analysis of a porous ceramic notched specimen under compressive creep loading. *Appl. Solid Mech.* **4,** 132–147.
Du, Z.-Z. and Cocks, A. C. F. (1992a). Constitutive models for the sintering of ceramic components—I. Material models. *Acta Metall.* **40,** 1969–1979.
Du, Z.-Z. and Cocks, A. C. F. (1992b). Constitutive models for the sintering of ceramic components—II. Sintering of inhomogeneous bodies. *Acta Metall.* **40,** 1981–1994.
FEMVIEW Limited (1989). FEMGEN/FEMVIEW manual.
Fleck, N. A., Kuhn, L. T. and McMeeking, R. M. (1992). Yielding of metal powder bonded by isostated contacts. *J. Mech. Phys Solids* **40,** 1139–1162.
Helle, A. S., Easterling, K. E. and Ashby, M. F. (1985). Hot isostatic pressing diagrams new development. *Acta Metall.* **26,** 2163–2174.
Hillert, M. (1965). Theory of normal and abnormal grain growth kinetics. *Acta Metall.* **13,** 227.
Hsueh, C. H., Evans, A. G., Cannon, R. M. and Brook, R. J. (1986). Visco elastic stresses and sintering damage in heterogeneous powder compacts. *Acta Metall.* **34,** 927–936.
Kuhn, L. T. and McMeeking, R. M. (1992). Power-law creep of powder bonded by isolated contacts. *Acta Metall.* **34,** 563–573.
McCoy, J. K. and Wills, R. R. (1987). Densification by interface-reaction controlled grain boundary diffusion. *Acta Metall.* **35,** 577–585.
McMeeking, R. M. and Kuhn, L. T. (1992). A diffusional creep law for powder compacts. *Acta Metall.* **40,** 961–969.
Pan, J. and Cocks, A. C. F. (1993). A constitutive model for stage 2 sintering of fine grained materials—II. Effects of an interface reaction. To be published.
Rahaman, M. N., De Jonghe, L. C. and Brook, R. J. (1986). Effect of shear stress on sintering. *J. Am. Ceram. Soc.* **69,** 53–58.
Rides, M., Cocks, A. C. F. and Hayhurst, D. R. (1989). *J. appl. Mech.* **56,** 493.
Shewmon, P. G. (1964). The movement of small inclusions in solids by a temperature gradient. *Trans Metall. Soc. AIME* **230,** 1134.

## APPENDIX: NEWTON–RAPHSON SCHEME

In this appendix we describe the Newton–Raphson scheme that was employed to solve eqns (26) and (34). Noting eqns (26) and (34), we set

$$g(\dot{\varepsilon}_e, \dot{\varepsilon}_v) = \frac{\partial \varphi}{\partial \dot{\varepsilon}_v} - \sigma_m + \sigma_s \tag{A1}$$

$$q(\dot{\varepsilon}_e, \dot{\varepsilon}_v) = \frac{\partial \varphi}{\partial \dot{\varepsilon}_e} - \sigma_e. \tag{A2}$$

For stage 1, we have

$$g(\dot{\varepsilon}_e, \dot{\varepsilon}_v) = \frac{c_r(\rho)}{3f_r(\rho)}\sqrt{\frac{L}{L_0}}\frac{\dot{\varepsilon}_v/3\dot{\varepsilon}_{0r}|\dot{\varepsilon}_v/3\dot{\varepsilon}_{0r}|}{\sqrt{f_r^2(\rho)(\dot{\varepsilon}_e/\dot{\varepsilon}_{0r})^3 + c_r^2(\rho)|\dot{\varepsilon}_e/3\dot{\varepsilon}_{0r}|^3}}\sigma_0 + \frac{1}{3f_b(\rho)}\left(\frac{L}{L_0}\right)^3\frac{\dot{\varepsilon}_v}{3\dot{\varepsilon}_{0b}}\sigma_0 - \sigma_m + \sigma_s \tag{A3}$$

and

$$q(\dot{\varepsilon}_e, \dot{\varepsilon}_v) = \frac{f_r(\rho)}{c_r(\rho)}\sqrt{\frac{L}{L_0}}\frac{(\dot{\varepsilon}_e/\dot{\varepsilon}_{0r})^2}{\sqrt{f_r^2(\rho)(\dot{\varepsilon}_e/\dot{\varepsilon}_{0r})^3 + c_r^2(\rho)|\dot{\varepsilon}_v/3\dot{\varepsilon}_{0r}|^3}}\sigma_0 + \frac{1}{c_b(\rho)}\left(\frac{L}{L_0}\right)^3\frac{\dot{\varepsilon}_e}{\dot{\varepsilon}_{0b}}\sigma_0 - \sigma_e. \tag{A4}$$

Differentiating these equations, we have

$$dg = \frac{\partial g}{\partial \dot{\varepsilon}_e}d\dot{\varepsilon}_e + \frac{\partial g}{\partial \dot{\varepsilon}_v}d\dot{\varepsilon}_v \tag{A5}$$

and

$$dq = \frac{\partial q}{\partial \dot{\varepsilon}_e} d\dot{\varepsilon}_e + \frac{\partial q}{\partial \dot{\varepsilon}_v} d\dot{\varepsilon}_v. \tag{A6}$$

Let

$$dg = 0 - g^i, \quad dq = 0 - q^i$$
$$d\dot{\varepsilon}_e^i = \dot{\varepsilon}_e^{i+1} - \dot{\varepsilon}_e^i, \quad d\dot{\varepsilon}_v^i = \dot{\varepsilon}_v^{i+1} - \dot{\varepsilon}_v^i,$$

where the superscript $i$ indicates the time increment.

We have

$$-g^i = \left(\frac{\partial g}{\partial \dot{\varepsilon}_e}\right)^i (\dot{\varepsilon}_e^{i+1} - \dot{\varepsilon}_e^i) + \left(\frac{\partial g}{\partial \dot{\varepsilon}_v}\right)^i (\dot{\varepsilon}_v^{i+1} - \dot{\varepsilon}_v^i) \tag{A7}$$

and

$$-q^i = \left(\frac{\partial q}{\partial \dot{\varepsilon}_e}\right)^i (\dot{\varepsilon}_e^{i+1} - \dot{\varepsilon}_e^i) + \left(\frac{\partial q}{\partial \dot{\varepsilon}_v}\right)^i (\dot{\varepsilon}_v^{i+1} - \dot{\varepsilon}_v). \tag{A8}$$

Solving these equations we find

$$\dot{\varepsilon}_v^{i+1} = \dot{\varepsilon}_v^i + \frac{q^i(\partial g/\partial \dot{\varepsilon}_e)^i - g^i(\partial q/\partial \dot{\varepsilon}_e)^i}{(\partial g/\partial \dot{\varepsilon}_v)^i(\partial q/\partial \dot{\varepsilon}_e)^i - (\partial q/\partial \dot{\varepsilon}_v)^i(\partial g/\partial \dot{\varepsilon}_e)^i} \tag{A9}$$

and

$$\dot{\varepsilon}_e^{i+1} = \dot{\varepsilon}_e^i + \frac{q^i(\partial g/\partial \dot{\varepsilon}_v)^i - g^i(\partial q/\partial \dot{\varepsilon}_v)^i}{(\partial g/\partial \dot{\varepsilon}_e)^i(\partial q/\partial \dot{\varepsilon}_v)^i - (\partial q/\partial \dot{\varepsilon}_e)^i(\partial g/\partial \dot{\varepsilon}_v)^i}. \tag{A10}$$

When $g^i$ and $q^i$ are both close to zero, say less than $10^{-3}$, we assume that $\dot{\varepsilon}_e^i$ and $\dot{\varepsilon}_v^i$ are the appropriate solutions. The relative density is then determined from the volumetric strain using the integrated form of eqn (4)

$$\rho = \rho_i \exp(-\varepsilon_{kk}). \tag{A11}$$

Similarly, for stage 2, we have

$$g(\dot{\varepsilon}_e, \dot{\varepsilon}_v) = \frac{1}{3} f_r^{-2/3}(\rho)\sigma_0 \frac{\sqrt{L/L_0}(\dot{\varepsilon}_v/3\dot{\varepsilon}_{0r})^{1/3}(|\dot{\varepsilon}_v/3\dot{\varepsilon}_{0r}|)^{1/3}}{[c_r^{-2/3}(\rho)(\dot{\varepsilon}_e/\dot{\varepsilon}_{0r})^{5/3} + f_r^{-2/3}(\rho)|\dot{\varepsilon}_v/3\dot{\varepsilon}_{0r}|^{5/3}]^{0.1}} + \frac{1}{3f_b(\rho)}\left(\frac{L}{L_0}\right)^3 \frac{\dot{\varepsilon}_v}{3\dot{\varepsilon}_{0b}}\sigma_0 - \sigma_m + \sigma_s \tag{A12}$$

$$q(\dot{\varepsilon}_e, \dot{\varepsilon}_v) = c_r^{-2/3}(\rho)\sigma_0 \frac{\sqrt{L/L_0}(\dot{\varepsilon}_e/\dot{\varepsilon}_{0r})^{2/3}}{[c_r^{-2/3}(\rho)(\dot{\varepsilon}_e/\dot{\varepsilon}_{0r})^{5/3} + f_r^{-2/3}(\rho)|\dot{\varepsilon}_v/3\dot{\varepsilon}_{0r}|^{5/3}]^{0.1}} + \frac{1}{c_b(\rho)}\left(\frac{L}{L_0}\right)^3 \frac{\dot{\varepsilon}_e}{\dot{\varepsilon}_{0b}}\sigma_0 - \sigma_e. \tag{A13}$$

Using the same procedure described above for stage 1, we obtain the roots of eqns (A12) and (A13) as $\dot{\varepsilon}_e^i$ and $\dot{\varepsilon}_v^i$.

For the transition stage, noting eqn (29), the deviatoric, the dilatational strain rate ($\dot{\varepsilon}_{et}$, $\dot{\varepsilon}_{vt}$) and the sintering potential, $\sigma_s$, were taken as

$$\dot{\varepsilon}_{et} = k\dot{\varepsilon}_{e\,\text{stage 1}} + (1-k)\dot{\varepsilon}_{e\,\text{stage 2}} \tag{A14}$$

$$\dot{\varepsilon}_{vt} = k\dot{\varepsilon}_{v\,\text{stage 1}} + (1-k)\dot{\varepsilon}_{v\,\text{stage 2}} \tag{A15}$$

$$\sigma_{st} = k\sigma_{s\,\text{stage 1}} + (1-k)\sigma_{s\,\text{stage 2}}. \tag{A16}$$